Electronic state and cage distortion in the room-temperature stable electride $[Ca_{24}Al_{28}O_{64}]^{4+}(O^{2-})_{2-x}(e^-)_{2x}$ as probed by ^{27}Al NMR

K. Matsuda,[1] Y. Konaka,[1] Y. Maniwa,[1,2] S. Matsuishi,[3] and H. Hosono[3,4]

[1]*Faculty of Science, Tokyo Metropolitan University, 1-1 Minami-osawa, Hachioji, Tokyo 192-0397, Japan*

[2]*CREST, JST, 4-1-8 Hon-Chou, Kawaguchi, Saitama 332-0012, Japan*

[3]*Frontier Research Center, Tokyo Institute of Technology, Mail-Box S2-13, 4259 Nagatsuta-cho, Midori-ku, Yokohama 226-8503, Japan*

[4]*Materials and Structures Laboratory, Tokyo Institute of Technology, Mail-Box R3-7, 4259 Nagatsuta-cho, Midori-ku, Yokohama 226-8503, Japan*

(Received 7 March 2009; revised manuscript received 10 September 2009; published 2 December 2009)

We report a microscopic study of the electronic states of the inorganic electride $[Ca_{24}Al_{28}O_{64}]^{4+}(O^{2-})_{2-x}(e^-)_{2x}$ ($x\sim0$, 1, and 2) by the ^{27}Al NMR technique. The ^{27}Al Knight shift as well as the Korringa behavior of the spin-lattice relaxation rate, T_1^{-1}, reveal a weak metallic character at one of two crystallographically inequivalent Al sites while insulating properties are exhibited at the other Al site on carrier doping, $x\sim1$ and 2. A detailed analysis of the Knight shift and Korringa values indicates that the Fermi-level density of states comes predominantly from the cage conduction-band electrons, proving the electronic states as electride for this material from the microscopic viewpoint. In addition, we find a decrease in an inverse of a product of T_1 and temperature below $T^*\sim40$ and 15 K for the electron-doped samples with $x\sim1$ and 2, respectively. This is explained by electron localization around the deformed cages due to the strong electron-lattice interaction at low temperatures.

DOI: 10.1103/PhysRevB.80.245103 PACS number(s): 71.20.−b, 81.05.Je, 76.60.−k, 61.72.−y

I. INTRODUCTION

$12CaO\cdot7Al_2O_3$ (C12A7) is a transparent insulator with a wide band gap of ~7 eV. The C12A7 cubic unit cell includes two chemical formulas and can be expressed as $[Ca_{24}Al_{28}O_{64}]^{4+}(2O^{2-})$.[1] The $[Ca_{24}Al_{28}O_{64}]^{4+}$ component represents a lattice framework, involving 12 cages with an inner space, ~0.4 nm in diameter (cf. Fig. 1). Each cage is connected directly to 12 other cages by sharing an oxide monolayer wall. The $2O^{2-}$ component is an extra framework of oxygen ions (hereinafter referred to as "free oxygen") that occupy two of 12 cages to maintain charge neutrality of the crystal. It has been found that electrons can be substituted, partially, or entirely for free oxygen to form $[Ca_{24}Al_{28}O_{64}]^{4+}(O^{2-})_{2-x}(e^-)_{2x}$, $(0\leq x\leq2)$.[2] This class of materials are referred to as inorganic electrides, in which electrons act as anions encaged in framework cations.[3] C12A7 is the first room-temperature stable electride and has attracted much attention owing to its peculiar electronic properties originating from a unique nanoporous structure.[4]

Upon removal of free oxygen, C12A7 undergoes an insulator-metal transition at the critical electron concentration $N_e\sim1\times10^{21}$ cm^{-3} $(x\sim1)$.[5] In the low electron-concentration region ($N_e\leq5\times10^{20}$ cm^{-3}, $x\leq0.5$), the optical reflectance spectra for C12A7 exhibits only Lorentz-type responses, showing that the encaged electrons are localized in the cages.[6] In the high electron-concentration region, both Drude-type and Lorentz-type responses are observed. This is thought to indicate the coexistence of localized electrons and free electron delocalized over the cages.

As for the electronic state in C12A7, several theoretical studies have been carried out in recent years.[7–11] *Ab initio* calculations using an embedded-cluster approach have revealed the existence of two types of conduction bands: "cage conduction band (CCB)" and "framework conduction band."[7] The framework conduction band is due to the cage framework while the CCB is related to three-dimensionally connected empty cages. The CCB is located about 2 eV below the bottom of the framework conduction band and is partially occupied in $[Ca_{24}Al_{28}O_{64}]^{4+}(4e^-)$. The CCB electrons tend to avoid the region occupied by the framework in this model and the CCB states can be viewed as linear combinations of *s*-like states formed inside the cages. Furthermore, it has been pointed out that framework distortion has a considerable effect on the CCB state electrons because of the strong electron-lattice interaction.[7,8]

These theoretical studies are particularly important in elucidating the mechanism of the superconductivity observed recently in $[Ca_{24}Al_{28}O_{64}]^{4+}(4e^-)$ at $T_C\sim0.4$ K.[12,13] However, experimental investigation of electronic states has largely been limited to macroscopic approaches such as resistivity, optical reflectance, and heat-capacity measurements,[4–6,12,13] and there is a strong need for more

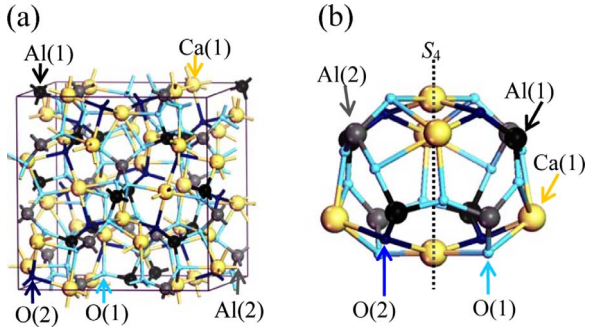

FIG. 1. (Color online) Crystal structure of C12A7. (a) Structure of the cage framework. Free oxygen in the cages is neglected for simplicity. The box shows a cubic unit cell containing 12 cages. (b) Structure of an empty cage of C12A7. The S_4 axis passes through two polar Ca ions and the cage center.

detailed confirmation of the novel electronic states of C12A7. In this context, we carried out a systematic study of $[Ca_{24}Al_{28}O_{64}]^{4+}(O^{2-})_{2-x}(e^-)_{2x}$ ($x \sim 0$, 1, and 2) using a local probe, ^{27}Al NMR over a wide temperature, T, range from 4.2 to 300 K, and report here the electronic state and the cage framework distortion of the electride C12A7. The present ^{27}Al NMR study revealed the very low electronic density of states around the Fermi level at the Al sites in the cage wall, showing that the electronic states at the Fermi level have a dominant contribution from the CCB electrons.

II. EXPERIMENT

The single crystals of C12A7 were grown by the Czochralski method. Each as-grown crystal was sealed in an evacuated quartz tube together with Ti metal and heated at 1100 °C to remove free oxygen. The sample preparation details have been reported elsewhere.[5] In the present study, two Ti-treated crystals (samples A and B) and an as-grown insulating crystal (sample C, $x \sim 0$) were employed for NMR measurements. The electron concentrations, as evaluated by optical-reflection measurements, were $\sim 2.3 \times 10^{21}$ cm^{-3} for sample A ($x \sim 2$) and $\sim 1.2 \times 10^{21}$ cm^{-3} for sample B ($x \sim 1$). Each crystal was pulverized in order to allow better rf penetration. Subsequently, the powder sample was placed inside a quartz NMR tube. The ^{27}Al NMR experiments were performed in an external field, H_0, of 9.4 T using a conventional phase-coherent pulsed spectrometer. The ^{27}Al NMR signal was detected by a $\pi/2$-τ-π spin-echo sequence. The typical $\pi/2$ pulse width was 3.0 μs. The ^{27}Al NMR spectra were taken by plotting the spin-echo signal intensity as a function of frequency at 9.4 T. The NMR shift was calculated with respect to the ^{27}Al resonance in a saturated $AlCl_3$ solution.

III. RESULTS AND DISCUSSION

A. ^{27}Al NMR spectra

Since the $I=5/2$ nuclear spin of ^{27}Al couples through its nuclear quadrupole moment, Q, to the electric field gradient (EFG) tensor $V_{\alpha\beta}$ created by its charge environment, the NMR spectrum consists of a broad line corresponding to the first-order quadrupole-perturbed satellite ($m = \pm 1/2 \leftrightarrow \pm 3/2$ and $\pm 3/2 \leftrightarrow \pm 5/2$) transitions and a narrow central line ($+1/2 \leftrightarrow -1/2$) quadrupole perturbed in second order. As can be seen in Fig. 2, the observed NMR line shape for sample A is composed of two sets of powder pattern spectra well articulated by nuclear quadrupolar splittings. One has a nuclear quadrupole frequency of $\nu_Q(1) = (3/20)eQV_{zz} = 1.63$ MHz and its asymmetry parameter $\eta(1) = |V_{xx}-V_{yy}|/V_{zz} \sim 0$ ($|V_{zz}| \geq |V_{yy}| \geq |V_{xx}|$). The other has $\nu_Q(2) = 0.48$ MHz and $\eta(2) \sim 0.26$. The full simulation of the spectrum shown in Fig. 2 agrees with the experimental results in nearly every detail. For the C12A7 framework, there are two crystallographically inequivalent Al sites, A1(1) and Al(2), which are tetrahedrally coordinated by four oxygen atoms and form AlO_4 tetrahedra. Al(1) forms a distorted tetrahedron with three bridging oxygen atoms and one nonbridging oxygen atom whereas the tetrahedron with Al(2)

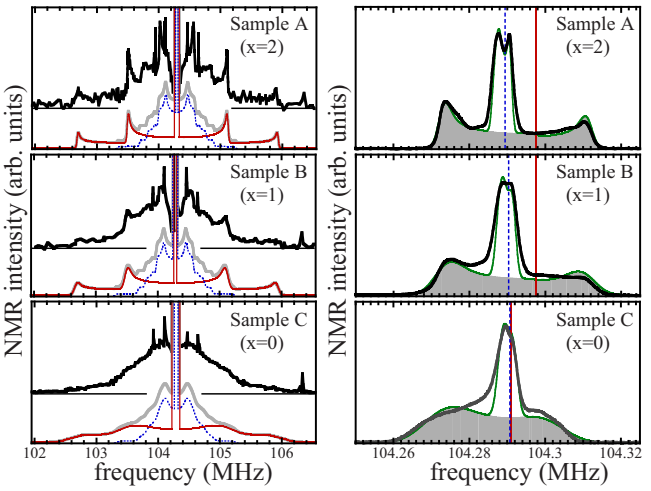

FIG. 2. (Color online) Left panel: ^{27}Al NMR satellite line shapes measured in samples A, B, and C at 293 K. The thick solid lines are the observed line shapes. The additional signal around 106.3 MHz is the ^{63}Cu NMR from the NMR coil. The solid gray lines represent the calculated line shapes. The thin solid and dotted lines are the calculated spectral components for Al(1) and Al(2), respectively. The calculated line shapes are convoluted with Gaussian functions. Right panel: ^{27}Al NMR ($m=+1/2 \leftrightarrow -1/2$) central transition spectra measured at 293 K. The spectra were taken by Fourier transforming the latter half of the spin-echo signal. The thin lines are calculated line shapes with $\nu_Q=1.63$ MHz and $\eta=0$ for Al(1), and $\nu_Q=0.48$ MHz and $\eta=0.26$ for Al(2). The line shapes are convoluted with Gaussian functions. The shaded parts represent the spectral components for Al(1). The solid and dotted vertical lines indicate the isotropic shift positions of Al(1) and Al(2), respectively.

is a normal tetrahedron with four bridging oxygen atoms.[1] We assigned the former and latter spectral components to Al(1) and Al(2), respectively, on the basis of the following experimental results: first, the spectral intensity ratio is in good agreement with the relative population ratio 4:3 of the Al(1) and Al(2) sites in the unit cell. Superposition of the two calculated line shapes of Al(1) and Al(2) in the weight ratio 4:3 gave the spectrum in Fig. 2. Second, ν_Q was expected to be larger for Al(1) than for Al(2) because the Al(1) tetrahedra are distorted. The present assignment of the spectrum is consistent with a previous ^{27}Al NMR study, in which the ^{27}Al central line shape was measured on a polycrystalline insulator.[14]

Theoretical calculation has revealed that the two polar Ca ions and one Al ion shift toward to the cage center due to the Coulomb interaction between the positively charged cage wall and the free oxygen which displaces from the S_4 axis (see Fig. 1).[8] The polar Ca ion shifts have been confirmed by recent synchrotron x-ray and neutron-diffraction experiments although no clear displacement of cage wall Al ions has been observed.[15–18] However, such a cage distortion would change the local environment of the Al sites, giving rise to broad distributions of the EFG parameters as well as NMR shifts of Al(1) and Al(2). Indeed, the line shapes of samples B and C with substantial free oxygen content are significantly broadened as compared to that of sample A. The central line shape,

which is well reproduced by the sum of the two spectra due to Al(1) and Al(2), is also smeared with increasing free oxygen occupancy. This indicates the elimination of cage distortion upon removal of free oxygen.

From the simulation of the central line shape, we extracted NMR isotropic shifts of Al(1) and Al(2) [hereafter denoted as $\delta(1)$ and $\delta(2)$, respectively] separately: $\delta(1)=146$ ppm and $\delta(2)=67$ ppm for sample A, $\delta(1)=144$ ppm and $\delta(2)=76$ ppm for sample B, and $\delta(1)=82$ ppm and $\delta(2)=80$ ppm for sample C. The measured shift is the sum of the chemical shift and Knight shift, K. The chemical shift is related to the orbital motion of the electrons, whereas the Knight shift is due to the hyperfine coupling of the nucleus to the conduction electrons. For the AlO_4 tetrahedron in common aluminates, the chemical shift is typically 50–90 ppm.[19] The values of $\delta(1)$ and $\delta(2)$ in sample C, which are in close agreement with the values given in Ref. 14, are within the ordinary chemical shift range. For samples A and B, $\delta(1)$ is too large to be explained solely in terms of chemical shift. Thus, the large values of $\delta(1)$ are attributed to the Knight-shift contribution. By assuming that the chemical shift of 82 ppm for Al(1) remains unchanged with free oxygen occupancy, the K of Al(1) was crudely estimated to be 74 and 72 ppm for samples A and B, respectively. This is two orders of magnitude smaller than the value of 1620 ppm for pure Al metal,[20] which indicates the very low electronic density of states (DOS) of Al s electrons at the Fermi level as discussed later with the T_1 results. Since, in contrast to $\delta(1)$, $\delta(2)$ decreases only slightly with decreasing free oxygen occupancy, $\delta(2)$ is practically determined by the chemical shift. Hence, the Fermi-level DOS at Al(2) is much smaller than that at Al(1).

B. ^{27}Al spin-lattice relaxation time

We now turn our attention to the ^{27}Al NMR spin-lattice relaxation rate, T_1^{-1}. The T_1^{-1} of Al(1) and Al(2) [hereafter denoted by $T_1^{-1}(1)$ and $T_1^{-1}(2)$, respectively] were measured by saturating the central transition ($m=+1/2\leftrightarrow-1/2$). The time-dependent recovery of the central line intensity for each Al site after saturation pulses was monitored. Since the observed NMR spectrum is well separated owing to the electric-quadrupole interaction, the recovery of ^{27}Al nuclear magnetization for central transition at time t after saturation pulses, $M(t)$, is properly given by the following multiexponential equation:

$$M(t) = M_0\left[1 - \frac{1}{35}\exp\left(-\frac{t}{T_1}\right) - \frac{8}{45}\exp\left(-\frac{6t}{T_1}\right) - \frac{50}{63}\exp\left(-\frac{15t}{T_1}\right)\right], \quad (1)$$

where M_0 is the magnetization under thermal equilibrium.[21] Typical recovery curves of nuclear magnetization for both sites at 100 K are shown in Fig. 3. The experimental result was confirmed to be fitted by Eq. (1) quite well and hence the precise T dependence of T_1^{-1} was obtained.

In Figs. 4(a)–4(c), we present the T dependence of $T_1^{-1}(1)$ and $T_1^{-1}(2)$ measured in samples A, B, and C, respectively.

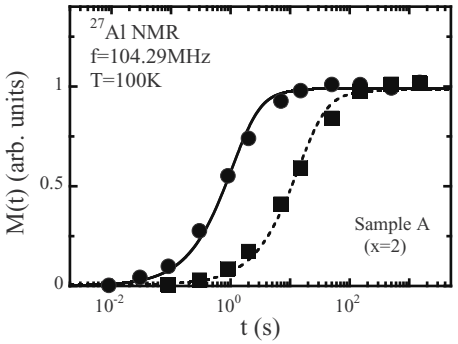

FIG. 3. Nuclear-magnetization recovery curves for the ^{27}Al central transition ($m=+1/2\leftrightarrow-1/2$) of Al(1) (closed circles) and Al(2) (closed squares) measured in sample A at 100 K. The lines in the figure are least-squares fits to Eq. (1) (see text). From these fits, the T_1 values were obtained to be 17.7 and 277 s for Al(1) and Al(2), respectively.

For sample C, $T_1^{-1}(1)$ and $T_1^{-1}(2)$ decrease nearly in proportion to T^7 with a $T_1(1)/T_1(2)$ ratio of ~1.7 down to ~100 K. Almost the same T dependence of $T_1^{-1}\propto T^7$ is observed in the $T_1^{-1}(2)$ of samples A and B above ~100 K. This is interesting because samples A and B are metallic while sample C is insulating.[5,13]

In contrast to $T_1^{-1}(2)$, $T_1^{-1}(1)$ is remarkably sample dependent, and exhibits a roughly linear T dependence below 150 K in samples A and B. It has been known that electron-doped samples have a finite DOS at the Fermi level.[5,13] Thus, the observed $T_1^{-1}\propto T$ behavior can be ascribed with confidence to the Korringa relaxation due to the conduction electrons in metals. On the other hand, above ~150 K $T_1^{-1}(1)$ shows a large deviation from the linear T dependence and a strong T dependence similar to those of insulating sample C and $T_1^{-1}(2)$ in metallic samples A and B. This suggests a cross-

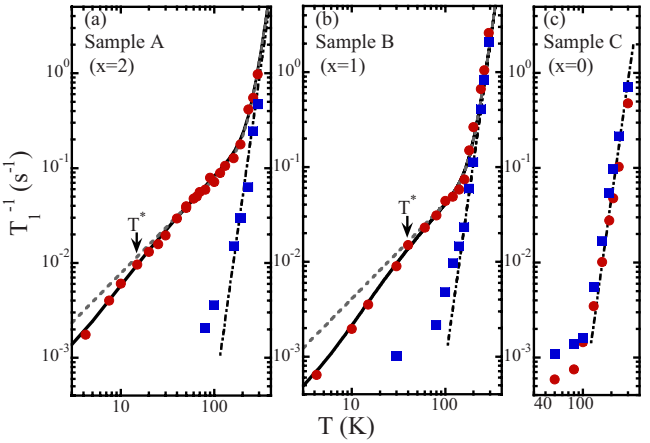

FIG. 4. (Color online) Temperature dependence of ^{27}Al nuclear-spin-lattice relaxation rate, T_1^{-1}, of Al(1) (closed circles) and Al(2) (closed squares): (a) in sample A, (b) in sample B, and (c) in sample C. The dash-dotted lines show $T_1^{-1}\propto T^7$. The dashed gray curves in (a) and (b) are least-squares fits of the data taken at higher temperatures to an equation of the form $T_1^{-1}=\alpha T+\beta T^7$, where α was assumed to be T independent. Then, the lines are extrapolated to the lower-temperature region. The solid lines correspond to fits of all the data points on the basis of Eq. (2)–(4) (see text).

over of the dominant relaxation mechanism from metallic to another type. To demonstrate such behavior, here, we assume that the experimental value of T_1^{-1} can be decomposed into two terms

$$T_1^{-1} = (T_1^{-1})_{cond} + (T_1^{-1})_{\text{extra}}. \quad (2)$$

Here, the first term represents the relaxation due to the coupling between nuclear spins and conduction-electron spins, and is given by

$$(T_1^{-1})_{cond} = 2hk_BT[\gamma_n H_{hf} D(E_F)]^2, \quad (3)$$

where h and k_B are the Planck constant and Boltzmann constant, respectively. γ_n is the ^{27}Al nuclear gyromagnetic ratio, H_{hf} is the hyperfine coupling, and $D(E_F)$ represents the DOS at the Fermi level. The second term represents contributions such as fluctuations of (i) the EFG at Al sites related to the phonons,[22–24] (ii) dipolar coupling with unpaired electrons in paramagnetic impurities, and (iii) nuclear dipolar coupling. The second term in Eq. (2) is tentatively assumed to be $(T_1^{-1})_{\text{extra}} \propto T^7$, which is expected for the nuclear-spin relaxation due to the two phonon Raman process at T values much lower than the Debye temperature.[22,23] In the insulating sample C, in which the conduction-electron part is negligible, the relaxation rate can be described very accurately by the T^7 dependence over 2 orders of magnitude as shown in Fig. 4.

The fits of the observed data with the above mentioned form $T_1^{-1} = \alpha T + \beta T^7$ are rather successful at T values above T^* as shown by the dashed gray lines in Fig. 4. The following parameters are obtained: $\alpha = 7.5 \times 10^{-4}$ s^{-1}K^{-1} and $\beta = 6.0 \times 10^{-18}$ s^{-1}K^{-7} for sample A, and $\alpha = 4.1 \times 10^{-4}$ s^{-1}K^{-1} and $\beta = 8.9 \times 10^{-18}$ s^{-1}K^{-7} for sample B. It is found that the results successfully describe the crossover in the dominant ^{27}Al relaxation process from the conduction-electron mechanism to another mechanism around 150 K. However, below T^*, $T_1^{-1}(1)$ starts to deviate from the linear T dependence again. This is more pronounced for the lightly doped sample B. We propose that this deviation is caused by a depression of DOS at low T; the α decreases with decreasing T. Fully fitted curves taking this effect into account are indicated by the solid lines in Fig. 4. More detailed discussions will be given later.

It is worth noting here that sample A has a larger α than sample B. This implies that the Fermi-level DOS increases with electron doping, which is consistent with the results of specific-heat measurements:[13] the electronic part of the specific heat or DOS at the Fermi level increases with x. This strongly supports the above-mentioned Korringa mechanism. We also note that the $(T_1T)^{-1}$ values obtained are three orders of magnitude smaller than the 5.6×10^{-1} s^{-1}K^{-1} measured in Al metal, showing a low Fermi-level DOS at Al(1). On the other hand, $T_1^{-1}(2)$ does not exhibit Korringa behavior down to $\sim$80 K even for the metallic samples A and B. This implies that the Fermi-level DOS at Al(2) is more than one order of magnitude smaller than the value for Al(1) in samples A and B. This is consistent with the Knight-shift results described previously.

Furthermore, we can obtain information on the electron correlation effect in conduction-electron system through the analysis of the so-called Korringa product, T_1TK^2. For the noninteracting conduction-electron systems, it is well known that the Korringa product is given by a constant: $S = (\gamma_e/\gamma_n)^2 h/(8\pi^2 k_B) = 3.89 \times 10^{-6}$ sK for ^{27}Al nucleus. However, in actual conduction-electron systems, the product is enhanced by $\kappa = T_1TK^2/S$ because of electron correlation effects.[20] Thus, we estimated κ from the observed T_1T and Knight shift K in the present experiments and obtained $\kappa = 1.4$ for sample A. This value lies in the range for ordinal simple metals.[20] This suggests that the electron correlation is not strong in this material.

We will now discuss the nature of electronic states at the Fermi level in detail, combining the present ^{27}Al NMR results with those of the previous specific-heat measurements. From the electronic specific-heat coefficient (γ), the DOS at the Fermi level, $D_\gamma(E_F)$, is obtained to be 6.1×10^{21} states eV^{-1} cm^{-3} for a metallic sample with $N_e \sim 2 \times 10^{21}$ cm^{-3}.[13] By taking the hyperfine coupling constant $H_{hf}^s = 1.9 \times 10^3$ kOe for Al metal, the Al s DOS around the Fermi level at Al(1) is evaluated to be 2.3×10^{19} states eV^{-1} cm^{-3} from Eq. (2). The evaluated Fermi-level DOS at Al(1) is only 0.38% of $D_\gamma(E_F)$. Furthermore, the Fermi-level DOS at Al(2) is much smaller than the value for Al(1). Hence, Al s states contribute little to the DOS at the Fermi level. This result is consistent with the nature of the CCB state: since electrons in the CCB tend to avoid the region occupied by the framework, the Fermi-level DOS of the Al s state becomes very low. On the other hand, the present result seems to be inconsistent with the framework conduction scenario in which the framework conduction bands are responsible for the electron transport because such a very low Fermi-level DOS at the Al sites would presumably interrupt the transport pathway.

Furthermore, evoking *ab initio* calculations based on an embedded-cluster approach,[7] in which the hyperfine interaction between the encaged electron and the ^{27}Al nuclei is specified not to exceed $H_{hf} = 13$ kOe, we can estimate the maximum limiting value for the observed $(T_1T)^{-1}$. Assuming $D_\gamma(E_F)$ is entirely attributable to the CCB states and using $H_{hf} = 13$ kOe, we obtain $\sim 5.3 \times 10^{-2}$ s^{-1}K^{-1} for the upper limit on $(T_1T)^{-1}$. This is much larger than the experimental values, 7.5×10^{-4} s^{-1}K^{-1} for Al(1) and $< 10^{-4}$ s^{-1}K^{-1} for Al(2). Therefore, the experimental results can be fully explained within a model of the Fermi level crossing the CCB.

Finally, we consider the decreasing behavior of $(T_1T)^{-1}$ below T^*, where $T^* \sim 15$ and ~ 40 K for samples A and B, respectively, as can be seen in Fig. 4. This suggests a decrease in the DOS at the Fermi level with decreasing T. The *ab initio* cluster calculation has confirmed that a cage occupied by an electron is deformed by a strong electron-lattice interaction. As a result, the encaged electron forms an F^+-centerlike state.[7,8] Indeed, optical-reflectance measurements at room temperature have revealed that electrons trapped in the cages coexist with conduction electrons in the CCB even in metallic samples with $N_e \geq 1 \times 10^{21}$ cm^{-3}.[6] This result is interpreted in terms of a model in which the bottom of the CCB is F^+-centerlike localized state induced by cage distortion due to the strong electron-lattice interaction and the delocalized states are superposed above these states. If a certain portion of the conduction electrons are also trapped at low T, the electronic states are modified, re-

sulting in a decrease in DOS at the Fermi level. Thus, we ascribe the deviation of T_1^{-1} below T^* to a decrease in the DOS at the Fermi level due to trapping of the CCB electrons in localized states.

In order to verify the above scenario, we employ the following simplest DOS model, which incorporates an activated process:

$$D(E_F) = \rho D_0 + (1-\rho)D_0 \exp\left(-\frac{\Delta E}{k_B T}\right), \quad (4)$$

where D_0 represents the limiting value of the Fermi-level DOS at high T and ρD_0 is the low T limiting value. ΔE is the activation energy characterizing the trap states. T_1^{-1} was calculated by using Eqs. (2)–(4). As demonstrated by the solid lines in Fig. 4, the T dependence of $T_1^{-1}(1)$ is successfully explained by taking the parameters $\rho=0.8$ and $\Delta E/k_B=15$ K for sample A and $\rho=0.6$ and $\Delta E/k_B=15$ K for sample B. As confirmed by the ^{27}Al NMR line-shape measurements, the framework is more severely distorted in sample B than in sample A. Since the local distortion of the framework perturbs the CCB states owing to the electron-lattice interaction, the deformed cages possibly act as electron-trap centers.[7,8] Hence, the Fermi-level DOS decreases more dramatically in sample B than in sample A, which leads to the smaller residual DOS (*viz.*, ρD_0) of sample B.

IV. SUMMARY

We have studied the electronic state of the first inorganic electride $[Ca_{24}Al_{28}O_{64}]^{4+}(O^{2-})_{2-x}(e^-)_{2x}$ ($x\sim 0, 1$, and 2) by ^{27}Al NMR. The ^{27}Al NMR line shapes due to Al(1) and Al(2) are sharpened upon removing the free oxygen, which confirms the elimination of cage distortion. The ^{27}Al Knight shift and Korringa behavior of T_1^{-1} reveal the weak metallic character at Al(1) while insulating properties are maintained at Al(2) on carrier doping ($x\sim 1$ and 2). A detailed analysis of the Knight-shift and Korringa values indicates that the Fermi-level DOS comes predominantly from the CCB electrons, proving the electronic states as electride for this material. In addition, we find a decrease in $(T_1T)^{-1}$ below $T^*\sim 40$ and 15 K for the electron-doped samples with $x\sim 1$ and 2, respectively. This is explained by the electron localization around the deformed cages at low T. However, the ^{27}Al NMR relaxation mechanism, which results in a $(T_1^{-1})_{\text{extra}} \propto T^7$ relationship for the "insulating" Al(2) site and the Al(1) site at high T, remains unclear.

ACKNOWLEDGMENTS

This work was supported in part by a Grant-in-Aid for Scientific Research by the Ministry of Education, Culture, Sports, Science and Technology of Japan.

[1] H. Bartl and T. Scheller, Neues Jahrb. Mineral., Monatsh. **35**, 547 (1970).
[2] S. Matsuishi, Y. Toda, M. Miyakawa, K. Hayashi, T. Kamiya, M. Hirano, I. Tanaka, and H. Hosono, Science **301**, 626 (2003).
[3] J. L. Dye, Science **301**, 607 (2003).
[4] H. Hosono, K. Hayashi, and M. Hirano, J. Mater. Sci. **42**, 1872 (2007).
[5] S. W. Kim, S. Matsuishi, T. Nomura, Y. Kubota, M. Takata, K. Hayashi, T. Kamiya, M. Hirano, and H. Hosono, Nano Lett. **7**, 1138 (2007).
[6] S. Matsuishi, S. W. Kim, T. Kamiya, M. Hirano, and H. Hosono, J. Phys. Chem. C **112**, 4753 (2008).
[7] P. V. Sushko, A. L. Shluger, K. Hayashi, M. Hirano, and H. Hosono, Phys. Rev. Lett. **91**, 126401 (2003).
[8] P. V. Sushko, A. L. Shluger, M. Hirano, and H. Hosono, J. Am. Chem. Soc. **129**, 942 (2007).
[9] J. E. Medvedeva and A. J. Freeman, Appl. Phys. Lett. **85**, 955 (2004).
[10] J. E. Medvedeva, E. N. Teasley, and M. D. Hoffman, Phys. Rev. B **76**, 155107 (2007).
[11] Z. Li, J. Yang, J. G. Hou, and Q. Zhu, Angew. Chem., Int. Ed. **43**, 6479 (2004).
[12] M. Miyakawa, S. W. Kim, M. Hirano, Y. Kohama, H. Kawaji, T. Atake, H. Ikegami, K. Kono, and H. Hosono, J. Am. Chem. Soc. **129**, 7270 (2007).
[13] Y. Kohama, S. W. Kim, T. Tojo, H. Kawaji, T. Atake, S. Matsuishi, and H. Hosono, Phys. Rev. B **77**, 092505 (2008).
[14] D. Müller, W. Gressner, A. Samoson, and E. Lippmaa, J. Chem. Soc., Dalton Trans. **1986**, 1277.
[15] T. Nomura, K. Hayashi, Y. Kubota, T. Kamiya, M. Hirano, M. Takata, and H. Hosono, Chem. Lett. **36**, 902 (2007).
[16] L. Palacios, A. G. De La Torre, S. Bruque, J. L. Garcia-Munoz, S. Garcia-Granda, D. Sheptyakov, and M. A. G. Aranda, Inorg. Chem. **46**, 4167 (2007).
[17] H. Boysen, M. Lerch, A. Stys, and A. Senyshyn, Acta Crystallogr., Sect. B: Struct. Sci. **63**, 675 (2007).
[18] R. Kiyanagi, J. W. Richardson, Jr., N. Sakamoto, and M. Yoshimura, Solid State Ionics **179**, 2365 (2008).
[19] *High-Resolution Solid-State NMR of Silicalites and Zeolite*, edited by G. Engelhardt and D. Michel (Wiley, New York, 1987).
[20] *Metallic Shift in NMR*, edited by G. C. Carter, L. H. Bennett, and D. J. Kahan (Pergamon, Oxford, 1977).
[21] A. Narath, Phys. Rev. **162**, 320 (1967).
[22] *The Principles of Nuclear Magnetism*, edited by A. Abragam (Oxford University Press, London, 1961).
[23] Y. Zhou, B. E. Bowler, G. R. Eaton, and S. S. Eaton, J. Magn. Reson. **139**, 165 (1999).
[24] If the nuclear-spin-lattice relaxation is dominated by a single-phonon (direct) process, T_1^{-1} is supposed to be proportional to H_0^2T. However, in the present case, the $T_1^{-1}(1)$ values measured in sample A are H_0 independent [$T_1^{-1}(1)=5.78\times10^{-2}$ and 5.93×10^{-2} s^{-1} for $H_0=4.0$ and 9.4 T at 80 K, respectively]. Furthermore, in a two-phonon Raman process, T_1^{-1} varies as T^n with the exponent n lying between 2 and 7. Hence, the behavior of $T_1^{-1}(1)\propto T$ at low T cannot be ascribed to the nuclear-spin-phonon relaxation.